Argonne
NATIONAL LABORATORY

ANL-AFCI-084

Development and Analysis of a Compact Low-Conversion Ratio Fast Burner Reactor

Nuclear Engineering Division

About Argonne National Laboratory

Argonne is a U.S. Department of Energy laboratory managed by The University of Chicago under contract W-31-109-Eng-38. The Laboratory's main facility is outside Chicago, at 9700 South Cass Avenue, Argonne, Illinois 60439. For information about Argonne, see www.anl.gov.

Availability of This Report

This report is available, at no cost, at http://www.osti.gov/bridge. It is also available on paper to the U.S. Department of Energy and its contractors, for a processing fee, from:

U.S. Department of Energy
Office of Scientific and Technical Information
P.O. Box 62
Oak Ridge, TN 37831-0062
phone (865) 576-8401
fax (865) 576-5728
reports@adonis.osti.gov

ANL-AFCI-084

Development and Analysis of a Compact Low-Conversion Ratio Fast Burner Reactor

by
M. A. Smith and R. N. Hill
Nuclear Engineering Division, Argonne National Laboratory

June 30, 2003

work sponsored by
U. S. Department of Energy,
Office of Nuclear Energy, Science and Technology

A U.S. Department of Energy laboratory managed by The University of Chicago

Advanced Fuel Cycle Initiative	**DOCUMENT RELEASE AUTHORIZATION**	

Argonne National Laboratory
9700 South Cass Avenue
Argonne, IL 60439

ANL AFCI Document Number:	ANL-AFCI-084	Release Date:	6/30/2003
Title:	Development and Analysis of a Compact Low-Conversion Ratio Fast Burner Reactor		
Author(s):	Micheal A Smith and Robert N. Hill		

Approval for Release

Approved by:			**Date**
Principal Author:	Micheal A Smith	Micheal A Smith	6/30/03
ANL Work Package Manager:	Robert N. Hill	Robert N. Hill	6/30/03
ANL Program Manager:	Phillip J. Finck	PF=Jr	6/30/03

Executive Summary

This report explores design options for compact fast burner reactors that can achieve low conversion ratios. Operational characteristics and whole-core reactivity coefficients are generated and contrasted with low conversion ratio designs of previous studies. A compact core point design is then selected and detailed reactivity coefficients are displayed and discussed.

The effectiveness of fast spectrum systems for actinide transmutation has been well documented. The key advantage of the fast spectrum resides in the severely reduced capture/fission ratios. This inhibits the production of the higher actinides that dominate the long-term radiotoxicity of nuclear waste. In conventional fast burner studies, the transmutation rate was limited by constraints placed on the fuel composition [1]. In an earlier phase of this study [2] the entire range of fuel compositions (including non-uranium fuel) was explored to assess the performance and safety limits of fast burner reactor systems. In this report, similar fuel compositions are utilized for application in compact configurations to achieve conversion ratios below 0.5.

The major design option explored to achieve a low conversion ratio is the reduction of fissile breeding by the removal of fertile material from the fast reactor system. To reduce the fertile content, the fuel pin diameter is decreased while the number of driver assemblies, the assembly size, and assembly pitch are held constant. This causes a reduction in the fuel volume fraction. In order to maintain criticality, the fissile loading must be conserved and thus reductions in the fertile content must be made.

Reactor performance parameters and reactivity coefficients were evaluated for four compact core configurations having conversion ratios ranging from 0.0 to 0.5. The results of these calculations show several trends with potential safety implications. Overall, the most important penalty incurred by the low conversion ratio is a significant increase in the burnup reactivity loss caused by the decrease in fissile breeding. Additionally, as the fuel pin diameter is decreased, the fuel enrichment and core leakage increase. Some key changes in the reactivity coefficients include a reduced sodium void worth (decreased and became negative) and a reduced Doppler coefficient (approaches zero).

A more rigorous investigation of the reactivity coefficients was performed. Typically, these coefficients are computed using diffusion theory, however, for high leakage systems, diffusion theory is known to breakdown significantly. For this reason, transport theory was implemented to verify the accuracy of the diffusion theory predictions of the reactivity coefficients. The sodium void worth was the only reactivity coefficient found to exhibit significant errors. These errors were overcome by modifying the cross section generation approach for this specific coefficient and a conservative estimate of the sodium void worth was obtained using diffusion theory.

In addition to the whole core reactivity coefficients, detailed spatial reactivity coefficients were generated and are discussed in this paper. These coefficients are intended for use in a rigorous safety analysis to be performed on the system point design. The general shape of and trends with the reactivity coefficient data were as expected and are consistent with previous results for fast burner reactor systems.

Development and Analysis of a Compact Low-Conversion Ratio Fast Burner Reactor

I. Introduction

On a basic level, the relative advantages of using a thermal or fast spectrum system for TRU transmutation can be determined by direct comparison of the capture/fission ratios of the two energy spectrums. For thermal systems, fission of the fertile isotopes such as U-238 is extremely small and thus the capture/fission ratio is very large (>100). For fissile isotopes like U-235 and Pu-239 the fission fraction in the thermal system is on the order of 65%. In contrast, for a fast spectrum system, fission accounts for nearly 90% of the absorptions for fissile isotopes (a capture/fission ratio of ~0.1) and the fission fraction for the fertile isotopes, dominated by U-238, is approximately 20% (~4 capture/fission ratio). The overall effect is that the production of actinides above Pu-239 is noticeably repressed in fast spectrum systems when compared to the thermal systems. These spectral effects allow the fast spectrum system to operate with better neutron efficiency and produce fewer higher actinides.

Another benefit of a fast spectrum system is its flexibility to manage TRU. To date, most fast reactors have been designed for fissile breeding; however, systems can readily be designed to operate as a TRU burner. The transmutation efficiency can be defined quantitatively by the TRU conversion ratio (CR)

$$TRU\ conversion\ ratio\ (CR) = \frac{TRU\ production\ rate}{TRU\ destruction\ (fission)\ rate}. \tag{1}$$

In traditional fast reactor systems, the focus was placed on loading more fertile material than was needed to operate the reactor thus allowing for breeding of fissile materials (in particular Pu-239 or U-233). Such fast breeder reactors were envisioned for a rapidly expanding nuclear power economy where fissile material was scarce and expensive. In terms of Eq. (1), these breeder reactors have conversion ratios greater than one (CR>1). For stabilization of the TRU content the conversion ratio is equal to one (CR=1).

In recent design studies [1], the focus has been placed on conversion ratios less than one (CR<1), referred to as fast burner reactors. This revised focus is motivated by the presence of excess weapons material, the existence of significant stockpiles of separated civil plutonium, and the potential improvements to repository management that TRU destruction can provide. Although conventional fast power reactor designs (e.g., CRBR, PRISM, EFR) were configured for fissile conservation (CR≥1), many of the demonstration reactors have actually been operated in a burner mode by removing the blanket regions; for example, the base FFTF configuration with full MOX loading yielded a CR of 0.4.

In Ref. 1, fast burner reactor designs were developed to operate at the limits of present day metal fuel technology allowing conversion ratios of 0.5 to 0.75. Although the focus was on disposition of weapons grade plutonium, the results are applicable to this work, where the disposition of recycled LWR fuel is studied. An additional study was performed in Ref. 1 using an exotic fuel form (non-uranium) in a conventional reactor design that allowed the reactor to achieve a 0.0 conversion ratio. A low Doppler reactivity coefficient and high sodium void worth were observed and a detailed safety assessment was not conducted. Given the undesirable

reactivity feedback features and development needs for a new fuel form, this pure burner option was deemed unattractive for short term deployment.

For the Advanced Fuel Cycle Initiative (AFCI) mission, the use of high leakage fast burner core designs to target conversion ratios from 0.0 to 0.5 was investigated last year [2]. In that report a simplified transient analysis was performed that indicated favorable passive safety behavior was retained for unprotected (beyond design basis) accidents. The main drawback of the approach in Ref. 2 was the use of a large diameter core (15 ft) that has significant economic penalties. This report compares the reactor performance data and reactivity coefficients of Ref. 2 to the results to a compact configuration with a much smaller core diameter (9 ft).

In Section II the details of the reactor physics models implemented for the design calculations are given while in Section III some parametric studies of low conversion ratio reactor designs are discussed. Because the high leakage configurations pose difficulties for diffusion theory, an examination of the reactivity coefficient predictions using transport theory is given in Section IV. Section V contrasts the reactor operating characteristics and reactivity coefficients for the high leakage and compact core designs. In Section VI, a system point design is chosen and detailed reactivity coefficients are presented.

II. Computational Models

The ANL suite of fast reactor analysis codes was used to evaluate reactor operating characteristics. Specifically, the MC^2-2, REBUS-3, VARI3D, DIF3D, and VIM codes were used. What follows is a brief description of each code and the task each code performs.

For standard multigroup calculations, a crucial part of the calculation is the method used to obtain the multigroup cross sections. Ideally, one would perform a whole core heterogeneous geometry calculation using thousands of energy groups, but such calculations are at present intractable. One must therefore rely upon more simplified approaches and focus on generating a set of coarse group, isotopic cross sections that accurately describe key reaction rates. Given the large range of achievable CRs, and thereby the large range of possible fuel enrichments, an essential component of cross section generation is the modeling of resonance self-shielding for fuel isotopes like U-238 and Pu-239.

MC^2-2 computes zero-dimensional flux solutions at a very fine energy structure for multigroup neutron cross section data and slowing-down spectra [3]. It performs explicit self-shielding corrections using cross section resonance parameters and a fast flux cross section library with more than 2000 energy groups. For this work, the MC^2-2 code is directly used to generate coarse group cross sections for the various reactor compositions (driver, reflector, control rod assemblies, etc...) using ENDF-V cross section data and resonance parameters.

In each reactor design, group constants were generated for four distinct zones: a low enrichment fuel zone, a high enrichment fuel zone, a reflector zone, and a shield zone. The ideal approach would be to use a representative spatial reactor geometry and perform the resonance self-shielding corrections and the group collapse for that geometry. The generation of such detailed cross section information would require not only resource intensive computations for each core configuration, but also, a companion analysis to determine the necessary sizing of the

spatial collapse and modeling accuracy of the heterogeneities would have to be performed. For this study a more simplified technique was employed.

For each fuel composition (one for each fuel enrichment zone), the MC^2-2 code is used to obtain regional group constants by performing an infinite medium critical buckling search (fundamental mode calculation). To obtain cross sections for the reflector zones, which have no fissile material, the leakage spectrum of the neighboring high enrichment zone is estimated and used as a fixed source within the reflector zone. Similarly, the cross sections for the shield zone are based upon an estimated leakage source taken from the adjacent reflector zone. Obviously this approach does not precisely account for the spatial variations of the spectrum within or between the various material zones; however, for fast reactor design calculations it has proven to be sufficient. Of particular importance is the proper handling of resonance self-shielding for the wide range of the compositions. For safety analysis, the same cross section generation procedure is used to obtain high temperature and voided sodium cross sections for the reactor compositions. The perturbed cross sections resulting in such accident conditions are used to calculate Doppler and sodium void worth coefficients as described later in this section.

REBUS-3 is a fuel cycle analysis code [4] for fast reactors which couples the DIF3D multigroup neutron flux code system [5] to a multigroup depletion code. In this work the enrichment search option of the REBUS-3 code is used to compute equilibrium cycle compositions for each reactor design. The necessary fuel enrichment and equilibrium discharge compositions (spent fuel composition) to assure criticality at EOEC are calculated for a specified TRU feed (recycled LWR transuranics), a base feed (depleted uranium), the reactor operating cycle (1 year with an 85% capacity factor as an example), and the fuel loading scheme (two enrichment zone with scatter loading, no shuffling, and fixed fuel residence time).

VARI3D is a neutron diffusion perturbation code [6] which makes use of the DIF3D code system. In this work the VARI3D code is used to compute the delayed neutron fraction, reactor kinetics parameters, and the reactivity worth coefficients necessary to assess the transient behavior of each reactor design. The six group kinetics parameters are generated from ENDF-V isotopic cross section data. The VARI3D code merges the kinetics data for all regions of the reactor and generates a single set of kinetics parameters for each reactor design. For reactivity coefficients involving dimensional changes, the finite difference or nodal transport option of the DIF3D code was used to perform direct calculations of the eigenvalue changes. The reactivity worth coefficients computed in this work are: sodium void coefficient, sodium, structure, and fuel density coefficients, flooded and voided Doppler coefficients, radial and axial fuel expansion coefficients, and a gas expansion module (GEM) worth.

The VARI3D code is also used to compute the sodium void worth and density reactivity coefficients. For the sodium void worth the exact perturbation worth of voiding (removing) of all of the flowing sodium within the fueled regions of the reactor and the plenum region above the active core is computed. It is important to note that specific cross sections were obtained for this accident condition by voiding the flowing sodium in the MC^2-2 calculations. Although this approach does not properly take into account the heterogeneity effects or the inherent transport effects associated with the sodium voiding, earlier work has shown that this approach provides a reasonable estimate of the sodium void effect. A similar composition modification is made to obtain the sodium density coefficient, but the cross sections obtained for the voided sodium

conditions are not used. The first order perturbation technique in VARI3D is used to obtain the reactivity worth for sodium density perturbation and the result is scaled appropriately to obtain a coolant density coefficient in cents/K. The fuel and structure densities are obtained by increasing the densities by some percentage (+10%) and using the first order perturbation option of the VARI3D code. The fuel and structure density results are also scaled to obtain coefficients in cents/K.

The calculation of the flooded and voided Doppler worths is also performed using the first order perturbation option of the VARI3D code. In this case, the perturbation does not involve any composition change, but instead, the material cross sections are perturbed in the flooded and voided configurations to reflect an increase in temperature. A doubling of the fuel, clad, and coolant temperatures is assumed and a reactivity coefficient is computed in cents/K.

To obtain reactivity worth coefficients for the radial and axial thermal expansions, a small dimensional change is made and the result is converted to cents/K (based on an appropriate thermal expansion coefficient). For the radial expansion coefficient, a uniform 1% expansion in the assembly pitch is assumed, the compositions and the geometry are modified appropriately, and a direct eigenvalue calculation is made using the finite difference diffusion option of the DIF3D code. For the axial expansion there are two possible contingencies to consider: axial expansion of the fuel and simultaneous axial expansion of the fuel and clad. For both approximations a 1% change in the active height is assumed, the compositions and geometry are modified appropriately, and eigenvalue calculations are carried out using the finite difference option of the DIF3D code.

To obtain data tables for input into the safety analysis code SAS4A [7], a FORTRAN utility code called TOSAS [8] is used to post process the VARI3D output. This utility code takes the perturbation solution and produces axial mesh perturbation worths for each assembly (or for groups of assemblies). The resulting data tables can then be converted directly into SAS4A input.

VIM is a Monte Carlo code that makes use of combinatorial geometry input and continuous energy cross section data [9]. In this work VIM is used to obtain estimates of the sodium void and GEM reactivity worths. Using a FORTRAN utility code called TOVIM [10] the DIF3D hexagonal geometry and assembly homogenized compositions are converted to VIM input and the microscopic cross sections are replaced with their ENDF-V continuous energy counter parts. In DIF3D, the fission products are treated using a lumped fission model. In VIM there was no lumped fission product available for this reactor system, thus it was decided that ^{99}Mo would be a reasonable approximation [11]. Direct eigenvalue differences were used to obtain whole core sodium void and GEM worths. This required that both the flooded and voided configurations be converted to VIM input and that relatively long Monte Carlo calculations be performed to obtain eigenvalues with small statistical errors. The resulting reactivity worths provide a comparison point for the DIF3D, VARI3D, and VIM codes.

III. Parametric Studies

The accuracy of the multigroup cross section generation techniques was verified in Ref. 2. The results of those parametric studies indicated that the fuel, coolant, and structure volume

fractions used in the cross section generation procedure should be consistent with those implemented in the fast reactor core design to avoid underestimation of the Doppler coefficient. Additional calculations were carried out using various refinements of energy group structure. Those results indicated that a 33 group cross section set would be sufficient to describe both the reactor operating characteristics and reactivity coefficients. The only major difference was observed in the sodium void worth discussed further in Section IV.

One of the conclusions reached in the parametric studies performed for Ref. 2, was that reactor geometry modifications (core radius to height modifications) alone could not reduce the conversion ratio below ~0.5. As a consequence, the investigation explored reduction of the fuel pin diameter as a means of reducing the conversion ratio further. In this study, reductions in the fuel pin diameter are employed as the sole means of reducing the conversion ratio for a compact core design. This allows low CRs to be attained with a compact configuration that has not been "spoiled" for high leakage.

To investigate the effects that pin diameter changes have upon the reactor performance parameters, calculations using a compact core (7 ring), a high leakage core (~12 rings) and a 11 ring core were performed (see Ref. 2 for descriptions of the high leakage and 11 ring core) and the results are given in Tables 1, 2, and 3. The fuel cycle analysis utilized the methods described in Section II. Fuel management was identical for each core, except the cycle length was reduced from 12 months to 6 months for the compact core configuration to obviate the high burnup swing.

Table 1. Pin Diameter Effect for the Compact Core Design.

Pin Diameter (cm)	**0.67**	**0.62**	**0.59**
Fuel Volume Fraction	0.30	0.24	0.22
TRU Enrichment (%)	30	39	49
BOC TRU Inventory (kg)	2221	2226	2235
Net TRU consumption rate (kg/yr)	122	161	193
Peak Linear Power (W/cm)	413	429	454
Ave. Discharge Burnup (MWd/kg)	112	143	177
Peak Discharge Burnup (MWd/kg)	209	263	321
Peak Fast Fluence (10^{23} n/cm^2)	3.9	3.9	4.0
Burnup Reactivity Loss (%dk)	2.6	3.5	4.3
TRU Conversion Ratio	**0.50**	**0.36**	**0.25**

As can be seen in Tables 1 through 3, as the fuel pin diameter is decreased, the fuel volume fraction decreases, the TRU enrichment increases, the net TRU consumption rate increases, and the TRU conversion ratio decreases. The TRU inventory for each core is rather constant over the range of pin diameters implemented with the minor variations seen attributable to the change in power distribution in the core and the hardening of the neutron energy spectrum. Also seen are substantial increases in the average and peak burnups as the fuel pin diameter decreases. These

changes are linked to the decrease in the total heavy metal fuel loading and are a consequence of producing the same amount of power with a smaller amount of material.

Table 2. Pin Diameter Effect for 11 Ring Core Design.

Pin Diameter (cm)	**0.74**	**0.70**	**0.65**	**0.60**	**0.55**
Fuel Volume Fraction	0.38	0.33	0.27	0.23	0.18
TRU Enrichment (%)	23	27	32	39	54
BOC TRU Inventory (kg)	3213	3189	3159	3141	3130
Net TRU consumption rate (kg/yr)	88	112	139	168	208
Peak Linear Power (W/cm)	269	270	271	272	280
Ave. Discharge Burnup (MWd/kg)	70	81	96	117	160
Peak Discharge Burnup (MWd/kg)	96	109	129	155	211
Peak Fast Fluence (10^{23} n/cm^2)	2.4	2.4	2.4	2.5	2.5
Burnup Reactivity Loss (%dk)	2.5	3.3	4.2	5.2	6.7
TRU Conversion Ratio	0.63	0.53	0.43	0.33	0.19

Table 3. Pin Diameter Effect for High leakage Core Design.

Pin Diameter (cm)	**0.74**	**0.70**	**0.65**	**0.60**
Fuel Volume Fraction	0.38	0.33	0.27	0.23
TRU Enrichment (%)	26	30	35	45
BOC TRU Inventory (kg)	3686	3653	3623	3602
Net TRU consumption rate (kg/yr)	108	130	156	189
Peak Linear Power (W/cm)	251	251	254	259
Ave. Discharge Burnup (MWd/kg)	67	78	93	119
Peak Discharge Burnup (MWd/kg)	90	104	123	156
Peak Fast Fluence (10^{23} n/cm^2)	2.2	2.2	2.3	2.3
Burnup Reactivity Loss (%dk)	2.7	3.4	4.2	5.2
TRU Conversion Ratio	0.55	0.46	0.37	0.26

From Tables 2 and 3 one can see that the high leakage core achieves the same conversion ratio as the 11 ring core design with a larger fuel pin diameter. More importantly, the high leakage core accomplishes this while reducing the burnup reactivity loss, the peak linear power, and the peak neutron fluence. Comparison of Table 1 to Table 3 shows that although the compact core can achieve the same conversion ratio as the high leakage core using the same pin diameter, it does so with several substantial penalties. In particular, the significant reduction in volume increases the peak linear power and decreases the TRU inventory. The lower TRU inventory exacerbates the reactivity loss rate requiring a shorter cycle length (6 months) to allow for a more reasonable reactivity control (rod worths).

IV. Transport Solutions of the Reactivity Coefficients.

One issue considered in this work is the inaccuracy in the reactivity coefficients caused by the limitations of diffusion theory. The fundamental reason for the failure of diffusion theory is its inability to properly model high leakage reactor configurations. Ideally, the application of transport theory to the same problem can indicate that such a problem exists and eliminate the inaccuracies. In this section, the reactivity coefficients calculated using transport theory are compared to those of diffusion theory. For brevity, only the EOC reactivity coefficients of the high leakage core will be considered.

The first reactivity coefficient investigated is the radial expansion coefficient, which is given in Table 4. The coefficients in Table 4 were obtained using the finite difference diffusion (FDD) option and the VARIANT [13], options of the DIF3D code system. The P_N levels represent the spherical harmonics expansion order used to represent the angular flux. As can be seen, the differences in diffusion theory and transport theory are insignificant for any of the four conversion ratio configurations.

Table 4. Radial Expansion Reactivity Coefficient (cents/K)

TRU Conversion Ratio	0.47	0.31	0.22	0.00
Beta	0.0032	0.0029	0.0028	0.0023
DIF3D FDD	-0.35	-0.41	-0.45	-0.58
VARIANT P_1	-0.35	-0.41	-0.45	-0.58
VARIANT P_3	-0.33	-0.38	-0.42	-0.55
VARIANT P_5	-0.32			-0.54

Next considered are the axial expansion coefficients. Table 5 gives the reactivity worth for 1% axial expansions calculated using FDD and VARIANT. There are two axial expansion cases that can occur: first, the fuel can expand within the clad (Fuel) and second, both the fuel and clad can expand together (Fuel and Clad). The "Fuel" worth is clearly larger in magnitude than the "Fuel and Clad" worth, however, in both cases the difference between transport theory and diffusion theory are insignificant. Overall, one can conclude that the radial and axial expansion reactivity coefficients are adequately modeled using diffusion theory.

Continuing with the sodium density coefficient, Table 6 gives the results computed using the VARI3D and VARIANT options of the DIF3D code system. Unlike the expansion coefficients, there are significant discrepancies between the diffusion and transport solutions of the sodium density coefficient. The 0.0 CR configuration in particular has a substantially larger error than the other CR configurations. The reason for the decreasing accuracy of the diffusion approach is believed to be a result of increased leakage in the core design for which diffusion theory is known to breakdown.

Table 5. Axial Expansion Reactivity Coefficient ($)

TRU Conversion Ratio	0.47	0.31	0.22	0.00
Fuel and Clad				
DIF3D FDD	-0.28	-0.33	-0.36	-0.45
VARIANT P_1	-0.27	-0.32	-0.35	-0.45
VARIANT P_3	-0.28	-0.34	-0.37	-0.48
VARIANT P_5	-0.28			-0.48
Fuel				
DIF3D FDD	-0.41	-0.45	-0.48	-0.55
VARIANT P_1	-0.41	-0.45	-0.48	-0.55
VARIANT P_3	-0.43	-0.48	-0.51	-0.60
VARIANT P_5	-0.43			-0.61

Table 6. Sodium Density Reactivity Coefficient (cents/K)

TRU Conversion Ratio	0.47	0.31	0.22	0.00
VARI3D	0.07	0.06	0.05	-0.08
VARIANT P_1	0.06	0.05	0.04	-0.10
VARIANT P_3	0.08	0.09	0.08	-0.01
VARIANT P_5	0.09			0.01

The next coefficient to consider is the GEM worth which measures the effect of voiding the GEMs. Table 7 gives the reactivity coefficients computed using the FDD and VARIANT options of the DIF3D module. Additional calculations were also performed using the continuous energy Monte Carlo code VIM. In all of the transport calculations seen in Tables 4 through 6, transport corrected isotropic scattering cross sections (S_0) were used. In the calculations that follow, both transport corrected isotropic scattering cross sections (S_0) and linear anisotropic scattering cross sections (S_1) are used. The GEM worth in Table 7 clearly displays a much larger error between diffusion and transport than that observed in the other coefficients. What is most important is that the VARIANT transport calculations agree with the VIM continuous energy calculations (using either S_0 or S_1 scattering), while the diffusion solutions do not. Although the transport approximation in VARIANT is clearly not converged (a higher order P_N flux expansion is required), the results obtained provide evidence of problems in the diffusion solution which can be corrected by using transport theory.

The last reactivity coefficient considered is the sodium void worth given in Table 8. In this calculation the flowing sodium is voided from the core and plenum regions. Again, VIM was used to obtain a continuous energy solution while the VARI3D and VARIANT codes were used to obtain deterministic results. What is most obvious in Table 8 is that both the transport and diffusion solutions do not agree with the VIM solution. The errors in the transport solutions are believed to be caused by problems with the cross section treatment in the voided configuration. In all of the preceding reactivity coefficients in this section, the neutron energy spectrum is assumed not to change significantly, thus the same cross sections were used for the unperturbed and perturbed cases. As a consequence, any systematic errors in the cross sections

would be present in both the unperturbed and perturbed calculations and would therefore cancel each other out. Given the accuracy of the GEM deterministic results this appears to be a valid assumption.

Table 7. Voided GEM Worth ($)

TRU Conversion Ratio	0.48	0.32	0.21	0.03
DIF3D FDD	-0.69	-0.88	-1.03	-1.40
VARIANT P_1 S_0	-0.80	-1.01	-1.18	-1.61
VARIANT P_3 S_0	-0.44	-0.56	-0.66	-0.90
VARIANT P_5 S_0	-0.37	-0.48	-0.56	-0.77
VARIANT P_1 S_1	-0.72	-0.90	-1.05	-1.39
VARIANT P_3 S_1	-0.41	-0.52	-0.60	-0.80
VARIANT P_5 S_1	-0.35	-0.45	-0.52	-0.70
VIM	-0.42 +/- 0.05	-0.36 +/- 0.06	-0.53 +/- 0.07	-0.80 +/- 0.08

Table 8. Voided Flowing Sodium Worth ($)

TRU Conversion Ratio	0.48	0.32	0.21	0.03
VARI3D	3.36	2.91	1.95	-2.99
VARIANT P_1 S_0	3.42	2.97	2.01	-2.98
VARIANT P_3 S_0	4.32	4.42	3.87	0.29
VARIANT P_5 S_0	4.57	4.82	4.37	1.15
VARIANT P_1 S_1	4.34	4.47	3.98	1.11
VARIANT P_3 S_1	4.75	5.16	4.88	2.75
VARIANT P_5 S_1	4.82	5.28	5.03	3.03
VIM	3.58 +/- 0.06	3.35 +/- 0.06	2.72 +/- 0.07	-2.15 +/- 0.08

In the sodium void worth, however, the impact on the neutron energy spectrum is too large and thus new cross sections had to be obtained for specific use in the voided configuration. Accordingly, one must assume that the generation and use of the "voided" cross sections would result in the same error with respect to the transport or "true" solution of the problem as that present in the "flooded" cross sections. The results from Table 8 seem to indicate that this assumption is not true. A comparison of VARIANT and VIM eigenvalues can demonstrate the problems with the cross section treatment. Table 9 gives the eigenvalues computed for the flooded and voided states of the 0.48 and 0.03 CR configurations. As can be seen, the VARIANT and VIM eigenvalue solutions for the 0.48 CR flooded state are very similar, but for the voided state the eigenvalues are substantially in error. This trend gets progressively worse as the CR is decreased to 0.03. In the 0.03 CR configuration not only is the voided eigenvalue off considerably, but so is the flooded eigenvalue.

For the sodium void worth in Table 8, the inaccuracies are a consequence of the dissimilar errors in the cross section generation procedure and their implementation into the

DIF3D model. To correct this problem, a closer inspection of the cross section treatment is needed to determine exactly which modeling approximation is causing the problem. A significant amount of effort was carried out trying to resolve the discrepancies, and in the end, a conservative estimate (when compared to the VIM prediction) of the void worth was obtained using diffusion theory.

Table 9. Flooded and Voided State Eigenvalues

	0.48 CR Configuration		0.03 CR Configuration	
	Flooded	**Voided**	**Flooded**	**Voided**
VARIANT P_1 S_0	0.9983	1.0093	0.9972	0.9901
VARIANT P_3 S_0	1.0139	1.0282	1.0169	1.0176
VARIANT P_5 S_0	1.0166	1.0319	1.0203	1.0231
VARIANT P_1 S_1	1.0188	1.0334	1.0300	1.0328
VARIANT P_3 S_1	1.0267	1.0429	1.0401	1.0473
VARIANT P_5 S_1	1.0276	1.0441	1.0413	1.0493
VIM	1.0278 +/- 0.0001	1.0400 +/- 0.0001	1.0363 +/- 0.0002	1.0307 +/- 0.0001

V. Low Conversion Ratio Design Description and Performance

Figure 1 shows the assembly layout for the high leakage reactor geometry of Table 3. This core consists of 162 high enrichment drivers and 192 low enriched drivers giving a total of 354 driver assemblies. There are 28 control rod positions, 3 alternate shutdown positions [2], and 12 GEMs. The diameter of the reactor is 4.44 m (14.6 ft) with an active core diameter of 3.38 m (11.1 ft) and an active height of 46 cm (18 in). The fuel assembly lattice pitch is 16.14 cm where each assembly consists of 271 fuel pins. For the base design (CR~0.5), the pin outside diameter is 7.44 mm with a pitch to diameter ratio of 1.19.

Figure 2 shows the assembly layout for the compact reactor geometry. This core consists of 60 high enrichment drivers and 42 low enriched drivers giving a total of 102 driver assemblies. There are 16 control rod positions and 3 alternate shutdown positions. No GEMs are utilized in this core design. The diameter of the reactor is 2.76 m (9.1 ft) with an active core diameter of 1.86 m (6 ft) and an active height of 113 cm (44 in). The fuel assembly lattice pitch is 16.14 cm where each assembly consists of 271 fuel pins. For the base design (CR~0.5), the pin outside diameter is 6.7 mm with a pitch to diameter ratio of 1.32.

Both cores are specified with an operating power of 840 MWt and an 85% capacity factor, but the high leakage core operates on a 12 month cycle while the compact core uses a 6 month cycle. Both cores also utilize seven batch loading schemes with an enrichment split of 1.25 (ratio of high to low enrichment) and a fast fluence limit of 4×10^{23} n/cm^2. The fluence limit was chosen based on FFTF operational data for the HT-9 alloy, the material chosen for cladding and subassembly structure. Reactor physics parameters for both reactors were generated for targeted conversion ratios of 0.5, 0.35, 0.25, and 0.0.

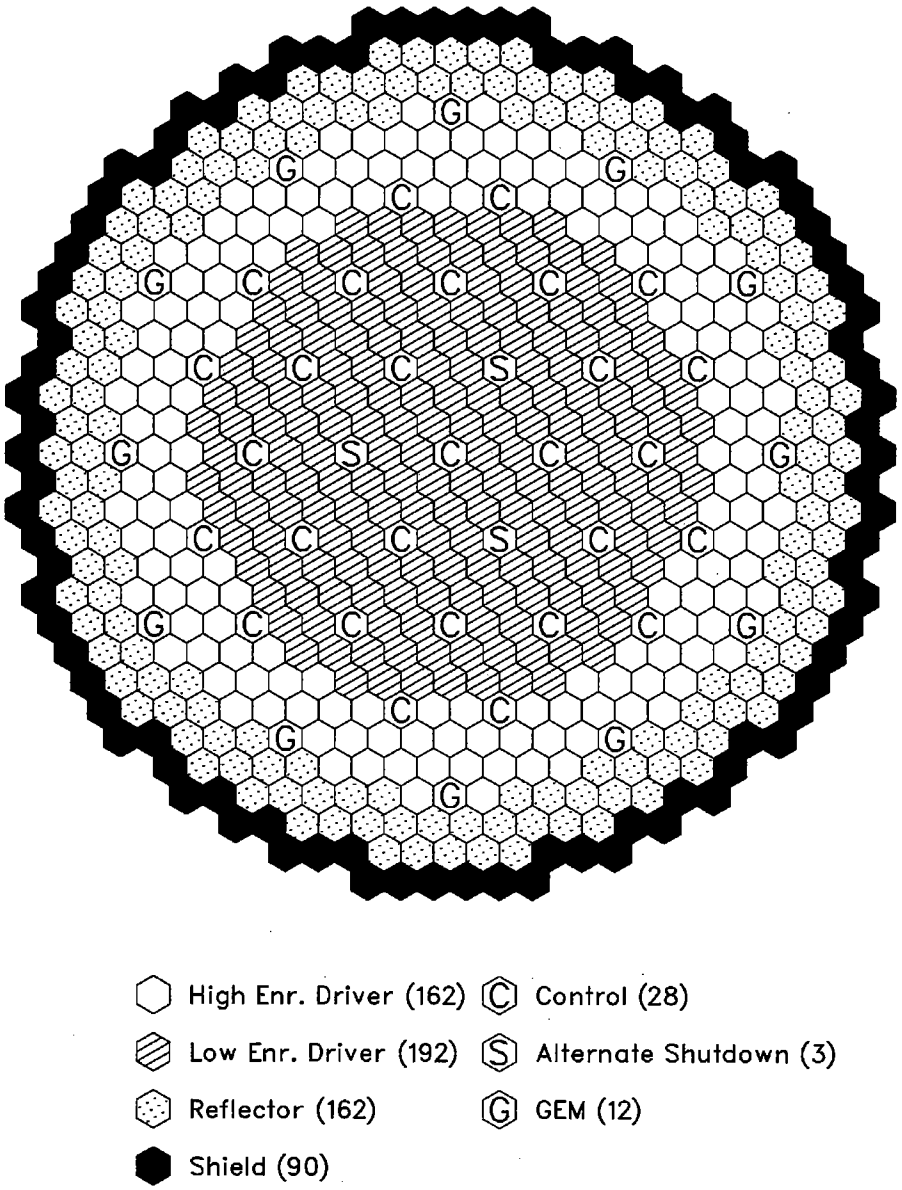

Figure 1. High leakage Core Configuration

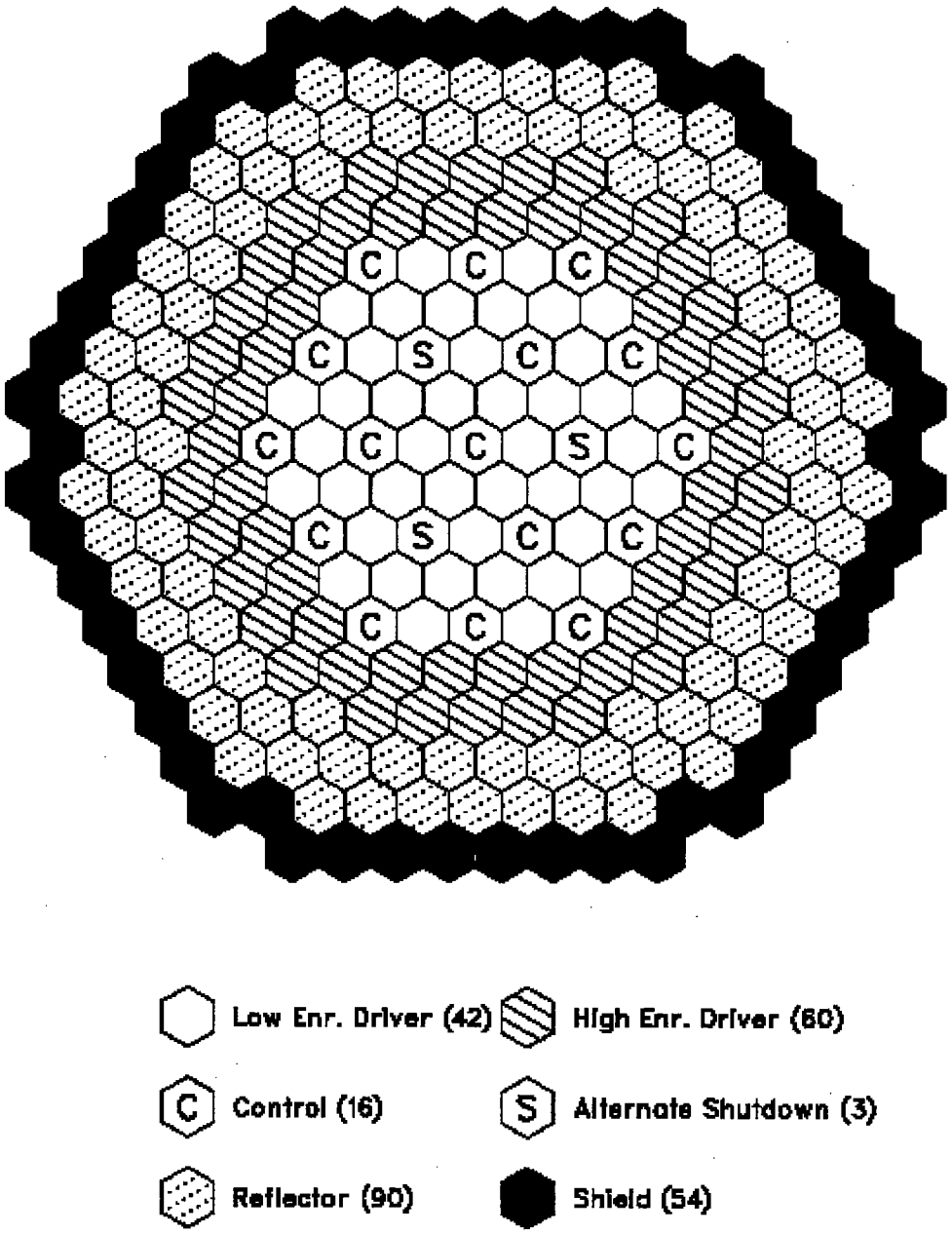

Figure 2. Compact Core Configuration

For each targeted low conversion ratio reactor a unique set of cross sections was generated following the procedure outlined in Section II. These cross sections were used to evaluate reactor performance parameters and reactivity worth coefficients. To avoid lower fuel melting temperatures caused by higher fuel enrichments of Pu, the Zr weight fraction was increased with increasing Pu enrichment. A maximum Zr fraction of 40% was used at 100% TRU/HM and is only relevant for the 0.0 CR case. Tables 10 and 11 give the reactor performance parameters of the two reactor cores at the four conversion ratio targets.

The most important trend seen in both Tables 10 and 11 is the large increase in burnup reactivity loss with reducing conversion ratio. The higher burnup reactivity losses are a direct result of the removal of fertile material from the reactor which is most clearly seen by the drop in total heavy metal inventory and relatively insignificant changes in the TRU inventory. To accomplish the complete removal of fertile uranium from the system the pin diameter must be dramatically decreased as observed. The use of a wire wrapped pin in either 0.0 CR design is unlikely and further assembly configuration changes (grid spacers) would be necessary to allow for such a pin diameter.

Table 10. High Leakage Core Reactor Performance Data for Different CR Reactors.

Targeted Conversion Ratio	**0.5**	**0.35**	**0.25**	**0.00**
Assembly Design Information				
Pin Diameter (cm)	0.74	0.67	0.64	0.49
Clad Thickness (cm)	0.06	0.06	0.06	0.06
Pitch/Diameter Ratio	1.19	1.32	1.40	1.83
Volume Fractions				
Fuel	0.38	0.30	0.26	0.14
Structure	0.25	0.26	0.27	0.33
Coolant	0.37	0.44	0.47	0.53
Low Enrichment Zone Enrichment	27	37	46	87
High Enrichment Zone Enrichment	33	46	58	93
Calculated REBUS-3 Reactor Parameters				
Calculated TRU Conversion Ratio	*0.47*	*0.31*	*0.22*	*0.00*
BOC Heavy Metal Loading (kg)	14219	10398	8372	4116
EOC Heavy Metal Loading (kg)	13951	10130	8104	3848
BOC TRU Loading (kg)	4156	4126	4127	4116
External Feed (kg/cycle)	2152	1609	1321	717
Net TRU consumption rate (kg/yr)	126	170	198	270
Peak Linear Power (W/cm)	271	284	293	325
Average Discharge Burnup (MWd/kg)	117	157	191	352
Peak Discharge Burnup (MWd/kg)	157	208	253	465
Peak Fast Fluence (10^{23} n/cm^2)	3.9	4.0	4.0	4.1
Burnup Reactivity Loss (%dk)	2.8	3.9	4.6	6.4

Table 11. Compact Core Reactor Performance Data for Different CR Reactors.

Targeted Conversion Ratio	0.5	0.35	0.25	0.00
Assembly Design Information				
Pin Diameter (cm)	0.67	0.62	0.59	0.45
Clad Thickness (cm)	0.06	0.06	0.06	0.06
Pitch/Diameter Ratio	1.32	1.44	1.51	1.96
Volume Fractions				
Fuel	0.30	0.24	0.22	0.12
Structure	0.26	0.28	0.28	0.35
Coolant	0.44	0.48	0.50	0.54
Low Enrichment Zone Enrichment	27	35	44	87
High Enrichment Zone Enrichment	33	44	56	93
Calculated REBUS-3 Reactor Parameters				
Calculated TRU Conversion Ratio	*0.50*	*0.36*	*0.25*	*0.00*
BOC Heavy Metal Loading (kg)	7485	5775	4571	2521
EOC Heavy Metal Loading (kg)	7351	5641	4437	2387
BOC TRU Loading (kg)	2254	2249	2250	2521
External Feed (kg/cycle)	1129	886	715	424
Net TRU consumption rate (kg/yr)	122	161	193	259
Peak Linear Power (W/cm)	413	429	454	513
Average Discharge Burnup (MWd/kg)	112	143	177	298
Peak Discharge Burnup (MWd/kg)	209	263	321	637
Peak Fast Fluence (10^{23} n/cm^2)	3.9	3.9	4.0	4.0
Burnup Reactivity Loss (%dk)	2.6	3.5	4.3	5.9

The whole-core reactivity coefficients for the high leakage core are tabulated at the beginning of cycle (BOC) and end of cycle (EOC) conditions in Table 12. Similarly, the whole-core reactivity coefficients for the compact core are tabulated in Table 13. As expected, when the pin diameter decreases and the uranium content decreases, there is a considerable decrease in the delayed neutron fraction (beta) and increase in the prompt neutron lifetime. Also, the Doppler coefficient decreases significantly. It is important to note, however, that the 0.25 CR designs still maintain a considerable fraction of the Doppler seen with the 0.50 CR designs. As for the decrease in beta, this will make the core more sensitive to small reactivity changes and additional consideration will have be given to normal operating transients. Overall, the changes in beta and Doppler can be attributed to the transition from a uranium dominated reactor system to a plutonium dominated system, as seen with the changes in zone enrichments in Tables 10 and 11.

Other important trends to observe in Tables 12 and 13 are increases in the expansion coefficients and GEM reactivity worths (high leakage core only) with a decreasing conversion ratio. These increases are caused by both the decrease in beta and the greater importance of

leakage for the lower conversion ratio reactor designs. The sodium density and sodium void reactivity coefficients also decrease with a decreasing conversion ratio. Although the magnitude of the sodium void coefficients may be in question, the relative change between the core designs is adequately modeled. The behavior of the sodium void and the sodium density coefficients can be traced to increased leakage caused by the altered fuel pin diameter (see discussion in Section II). In particular, the transition to negative sodium void and density reactivity worths in the 0.00 CR configuration are a direct result of the substantial amount of neutron leakage introduced into the system (compare the coolant volume fractions of the reactor configurations in Table 10 and 11).

Table 12. Reactivity Worth Coefficients for the High Leakage Core

Calculated Conversion Ratio	0.47	0.31	0.22	0.00
BOC				
Beta	3.18E-03	2.92E-03	2.75E-03	2.28E-03
Prompt Neutron Lifetime	3.29E-07	3.73E-07	3.98E-07	4.97E-07
Sodium Density Worth (cents/K)	0.06	0.05	0.03	-0.11
Sodium Void Worth ($)	2.95	2.35	1.35	-3.12
Radial Expansion Worth (cents/K)	-0.36	-0.42	-0.53	-0.60
Axial Expansion Coefficient				
Fuel & Clad (cents/K)	-0.17	-0.21	-0.24	-0.33
Fuel (cents/K)	-0.19	-0.23	-0.26	-0.34
Doppler (cents/K)	-0.064	-0.048	-0.037	-0.010
Control Rod Driveline Expansion ($/cm)	-0.79	-1.00	-1.16	-1.63
GEM Worth ($)	-0.39	-0.49	-0.57	-0.83
EOC				
Beta	3.17E-03	2.92E-03	2.76E-03	2.31E-03
Prompt Neutron Lifetime	3.52E-07	4.07E-07	4.41E-07	5.70E-07
Sodium Density Worth (cents/K)	0.07	0.06	0.05	-0.09
Sodium Void Worth ($)	3.36	2.91	1.95	-2.99
Radial Expansion Worth (cents/K)	-0.34	-0.40	-0.44	-0.57
Axial Expansion Coefficient				
Fuel & Clad (cents/K)	-0.11	-0.13	-0.15	-0.21
Fuel (cents/K)	-0.13	-0.16	-0.17	-0.22
Doppler (cents/K)	-0.066	-0.060	-0.051	-0.011
Control Rod Driveline Expansion ($/cm)	-0.77	-0.96	-1.09	-1.59
GEM Worth ($)	-0.37	-0.46	-0.54	-0.80
Burnup Reactivity Loss ($)	8.89	13.40	16.64	27.72

Table 13. Reactivity Worth Coefficients for the Compact Core

Calculated Conversion Ratio	0.50	0.36	0.25	0.00
BOC				
Beta	3.13E-03	2.92E-03	2.76E-03	2.44E-03
Prompt Neutron Lifetime	3.60E-07	4.01E-07	4.35E-07	5.18E-07
Sodium Density Worth (cents/K)	0.13	0.12	0.10	-0.01
Sodium Void Worth ($)	5.6	4.9	3.8	-1.6
Radial Expansion Worth (cents/K)	-0.31	-0.35	-0.39	-0.47
Axial Expansion Coefficient				
Fuel & Clad (cents/K)	-0.23	-0.28	-0.32	-0.40
Fuel (cents/K)	-0.26	-0.31	-0.34	-0.43
Doppler (cents/K)	-0.070	-0.061	-0.047	-0.001
Control Rod Driveline Expansion ($/cm)	-0.54	-0.69	-0.81	-1.11
EOC				
Beta	3.11E-03	2.92E-03	2.77E-03	2.47E-03
Prompt Neutron Lifetime	3.79E-07	4.29E-07	4.71E-07	5.80E-07
Sodium Void Worth ($)	6.3	5.7	4.8	-0.7
Sodium Density Worth (cents/K)	0.15	0.14	0.13	0.03
Radial Expansion Worth (cents/K)	-0.29	-0.32	-0.35	-0.42
Axial Expansion Coefficient				
Fuel & Clad (cents/K)	-0.22	-0.25	-0.28	-0.35
Fuel (cents/K)	-0.25	-0.28	-0.31	-0.38
Doppler (cents/K)	-0.076	-0.067	-0.052	0.000
Control Rod Driveline Expansion ($/cm)	-0.48	-0.58	-0.66	-0.89
Burnup Reactivity Loss ($)	8.32	12.04	15.44	23.90

Another important coefficient to consider is the control rod driveline expansion coefficient, which is pertinent to certain accident conditions like severe earthquakes. In these accidents the potential exists for relative motion between the core and control rods leading to large insertions of reactivity. As can be seen the control rod driveline expansion increases sharply as the conversion ratio decreases for either the compact or high leakage cores, but the high leakage core clearly has a larger magnitude. The reason for the larger magnitude in the high leakage core is the reduced height. Although the transient analysis carried out in Ref. 2 has shown the effect to be manageable for the high leakage core, earthquake type accidents were not considered in that work.

The most important difference between the high leakage and compact core designs is seen in the peak linear power of Tables 10 and 11 and the sodium void worth of Tables 12 and 13. The large increase in the peak linear power is a result of the compact core utilizing a smaller amount of fuel to produce the same amount of power. Increasing the fuel pin height of the compact core does not help since that would also increase the conversion ratio. As for the

sodium void worth, the compact core design severely reduces axial leakage resulting in a more positive void worth. The only way to decrease the sodium void worth is to increase the core diameter to height ratio or to artificially introduce more leakage into the core during the accident scenario.

Overall, the lower fuel inventory and core diameter of the compact core make it more desirable, even though the peak linear power and sodium void worth are higher. Although increasing the core diameter can lessen the problems with the peak linear power and sodium void worth, demonstrating that the compact core can perform safely is more beneficial. For, if the compact core can be shown to behave safely, it would be clear that a slightly larger diameter core would also behave in a safe manner. The 0.0 CR configuration of the compact core design is not plausible because of the uncertainties in the fuel composition feasibility and assembly geometry. As a result, the 0.25 CR compact core configuration was chosen as the system design and more detailed reactor performance characteristics and reactivity coefficients were obtained.

VI. 0.25 CR Compact Core System Point Design

The compact core geometry for the 0.25 CR configuration is the same as that discussed in the preceding sections including the fuel pin diameter which was fixed for this point design. The 6 month operating cycle and power level are also maintained. In the point design model a recycle scenario is included in addition to the startup scenario studied thus far. In the startup scenario, the "startup" of the reactor using recycled LWR fuel as the enrichment feed is considered since a significant quantity of the recycled LMR would not be present. In the recycle scenario the spent LMR fuel is assumed to be recycled with appropriate losses and the recovered TRU is then used as the primary external feed with the recycled LWR feed used as makeup enrichment feed. A recycled uranium contaminant is also added to the recycled LWR fuel to simulate a more realistic reprocessing scenario.

First considered are the reactor performance characteristics given in Table 14. As can be seen, the startup results are nearly identical to those given in Table 13 earlier, even though the LWR feed was changed (inclusion of the uranium contaminant). The major differences between the startup and recycle scenarios can be seen in the zone enrichments. Since the fuel pin diameter was held constant, the enrichment feed effectively changes to an isotopic mix slightly worse than that of the original recycled LWR enrichment [14]. As a consequence, a higher enrichment is needed in the recycle scenario even though the heavy metal inventory doesn't change. Because of the degraded enrichment feed and higher enrichment, the conversion ratio drops from 0.25 to 0.19. Additionally, the change in the enrichment feed and enrichment also impact fissile breeding causing the peak discharge burnup, peak linear power, and burnup swing to decrease.

Next considered are the whole-core reactivity coefficients given in Table 15 for BOC and EOC. Most of the reactivity coefficients are nearly identical between the startup and recycle scenarios. There is, however, a significant decrease in the delayed neutron fraction and increase in the sodium void worth. Both of these are a result of the degraded isotopic fuel content and the increased enrichment. The EOC VIM void worth solution is also given to demonstrate the improvement in the sodium void worth predicted using diffusion theory. Now the diffusion

results are only slightly larger than the continuous energy calculation and pose a conservative estimate of the void worth.

Table 14. Compact Core Reactor Performance Data for the 0.25 System Point Design.

	Startup	Recycle
Calculated TRU Conversion Ratio	**0.25**	**0.19**
Cycle Length (months)	6.00	6.00
Assembly Residence Time (full-power days)	1086	1086
Low Enrichment Zone Enrichment	44	55
High Enrichment Zone Enrichment	56	68
BOC Heavy Metal Inventory (kg)	4571	4564
EOC Heavy Metal Inventory (kg)	4437	4430
BOC TRU Loading (kg)	2250	2806
Recycled HM Feed (kg/yr)	0	1158
Recycled Uranium (kg/yr)	0	478
External HM Feed (kg/yr)	1430	269
External Uranium (kg/yr)	701	57
Total HM Feed (kg/yr)	1430	1427
Net TRU consumption rate (kg/yr)	193	211
Average Discharge Burnup (MWd/kg)	177	177
Peak Discharge Burnup (MWd/kg)	321	254
Peak Linear Power (W/cm)	454	433
Peak Fast Fluence (10^{23} n/cm^2)	4.0	3.9
Burnup Reactivity Loss (%dk)	4.3	3.5

Table 15. Compact Core Reactivity Coefficients for the 0.25 System Point Design.

	Startup	Recycle
TRU Conversion Ratio	0.25	0.19
BOC		
Beta	2.76E-03	2.57E-03
Prompt Neutron Lifetime	4.35E-07	4.15E-07
Sodium Density Worth (cents/K)	0.10	0.16
Sodium Void Worth ($)	3.83	6.12
Radial Expansion Worth (cents/K)	-0.39	-0.41
Axial Expansion Coefficient		
Fuel & Clad (cents/K)	-0.32	-0.32
Fuel (cents/K)	-0.34	-0.36
Control Rod Driveline Expansion ($/cm)	-0.81	-0.78
Doppler (cents/K)	-0.047	-0.034
EOC		
Beta	2.77E-03	2.59E-03
Prompt Neutron Lifetime	4.71E-07	4.49E-07
Sodium Density Worth (cents/K)	0.13	0.18
Sodium Void Worth ($)	4.85	6.61
VIM Sodium Void Worth ($)	4.37 +/- 0.07	6.42 +/- 0.07
Radial Expansion Worth (cents/C)	-0.35	-0.37
Axial Expansion Coefficient		
Fuel & Clad (cents/K)	-0.28	-0.29
Fuel (cents/K)	-0.31	-0.33
Control Rod Driveline Expansion ($/cm)	-0.66	-0.62
Doppler (cents/K)	-0.052	-0.038
Burnup Reactivity Loss ($)	15.44	13.69

The spatial details of the reactivity coefficients which are used in the safety analysis code SAS4A were evaluated by assigning several assemblies with similar compositions and power levels to a thermal-hydraulic channel. The lumping scheme used in this work is shown in Figure 3 where the numbers represent thermal-hydraulic channel number assigned to each assembly. Each reactivity coefficient is then plotted axially through the core for each channel. For this analysis only the EOC recycle reactivity coefficients are displayed.

Figures 4 and 5 give an axial plot of the fuel density and structure density reactivity worths, respectively. In the fuel density calculation the density of the fuel (transuranics, zirconium, and fission products) is assumed to increase and, as a consequence, positive reactivity is inserted into the core. As one would expect, there is a large peak in the reactivity worth at the core center. This effect is seen in both the radial direction and the axial direction. In Figure 5, the density of the cladding and structural materials (Fe, Cr, Co, etc...) is assumed to increase, thereby increasing the parasitic absorption. As expected, the structure density worth displays a trend similar to that of the fuel density, except it is negative.

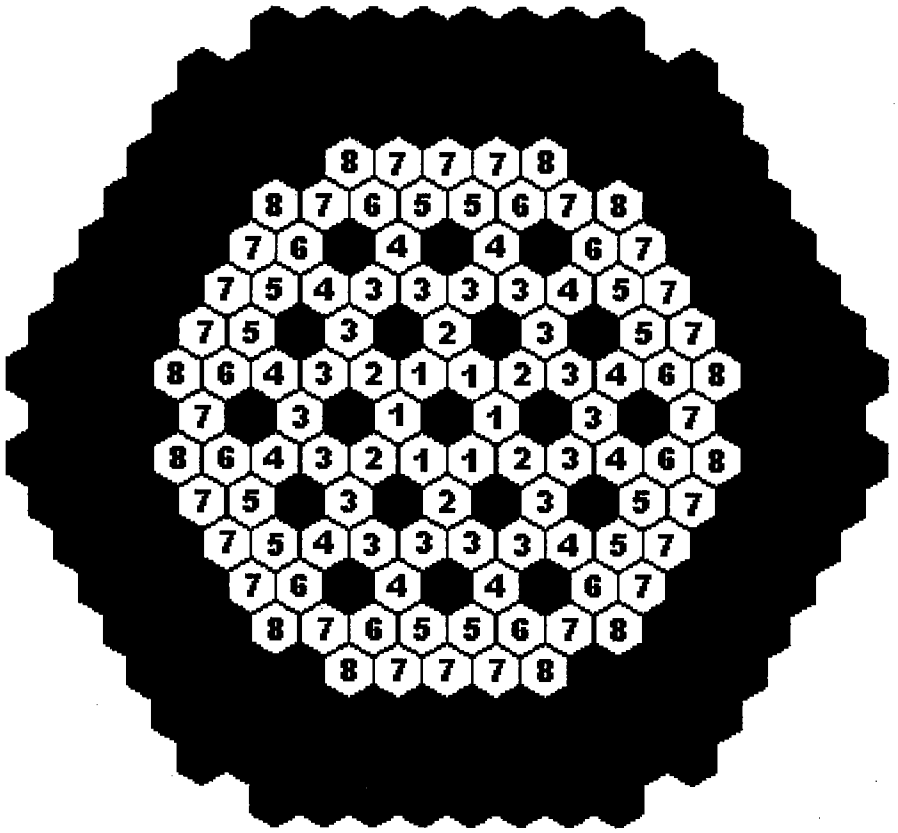

Figure 3. Thermal-Hydraulic Channel Assignment For Driver Assemblies

Figure 6 and 7 give the axial plots of the sodium density and sodium void reactivity worths, respectively. For the sodium density calculation, the density of the sodium is assumed to decrease which leads to a harder energy spectrum and a larger number of neutrons produced per absorption. The reactivity worth is therefore positive. Similarly, in the sodium void calculation the flowing sodium is assumed to void leading to a large positive reactivity insertion. Both coefficients have a more pronounced reactivity effect near the center of the core than at the periphery as that seen in the fuel and structure density reactivity coefficients. In this case, however, both the sodium density coefficient and sodium void worth become negative at the core periphery which is a result of the increased leakage of the harder spectrum neutron flux.

An axial plot of the flooded Doppler reactivity worth is given in Figure 8. In this calculation, the temperature of the fuel, cladding, and coolant is assumed to increase. What is most obvious is the peaking of the Doppler worth curve at the axial edges of the active core. This is a spectral effect caused by reflection of lower energy neutrons back into the core. Because of the different volume fractions of structural and sodium above and below the core (above the active core the fuel pin plenum takes a substantial amount of volume) the effect is more pronounced for the lower reflector yielding the asymmetry observed in Figure 8.

Finally, Figure 9 gives an axial plot of the voided core Doppler reactivity worth. In this calculation the flowing sodium is assumed to be voided and the same increase in the fuel, structure, and coolant temperatures is made. This coefficient has a distribution similar to that of the flooded Doppler but the values are clearly more negative. The outer channels also have a significant negative dip near the center of the active core region which is caused by the radial steel reflectors. These reflectors soften the spectrum similar to that seen with the axial reflector below the core. The reflector interaction is more pronounced in the voided Doppler coefficient because of the increased leakage resulting from the voided sodium.

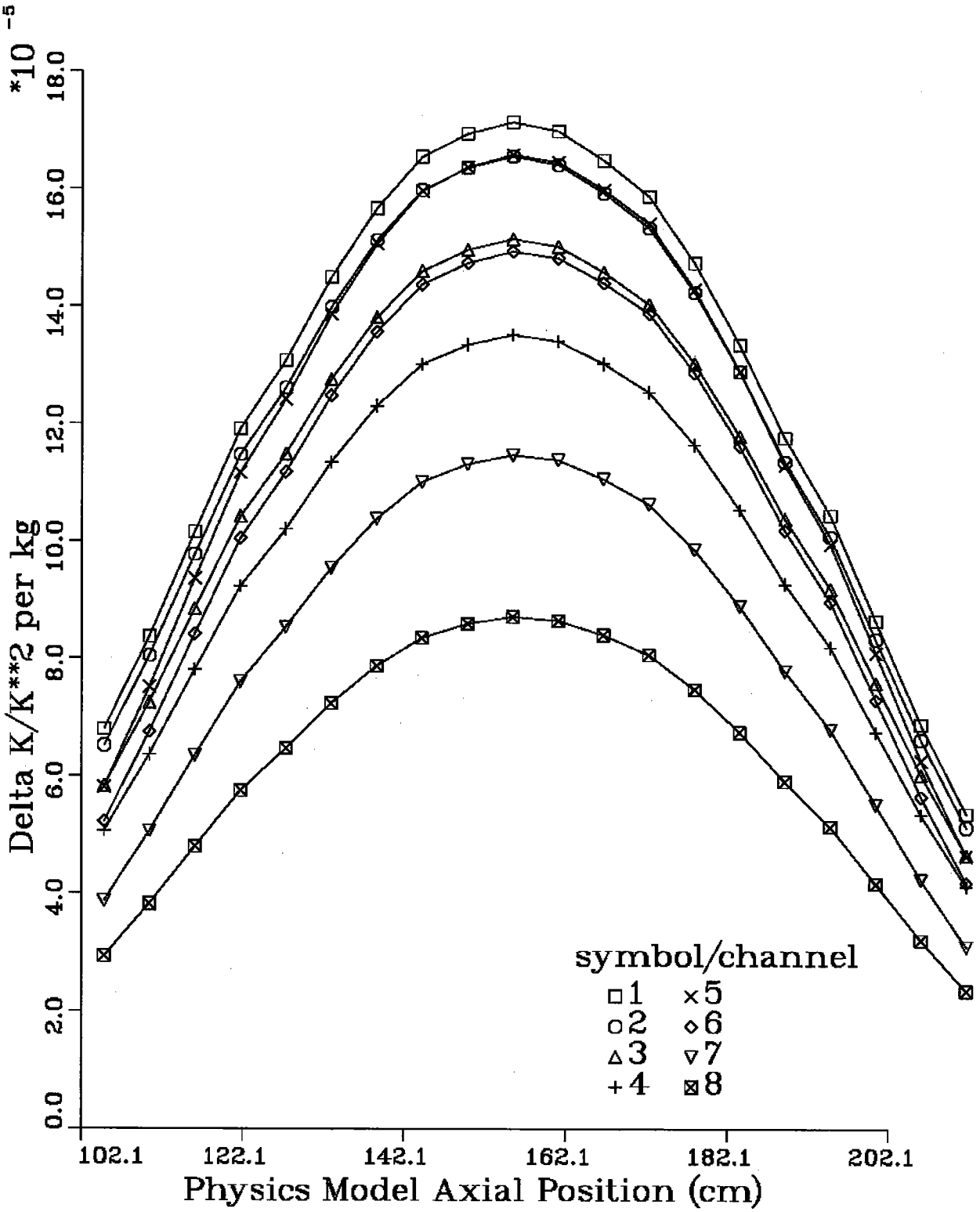

Figure 4. Fuel Density Worth

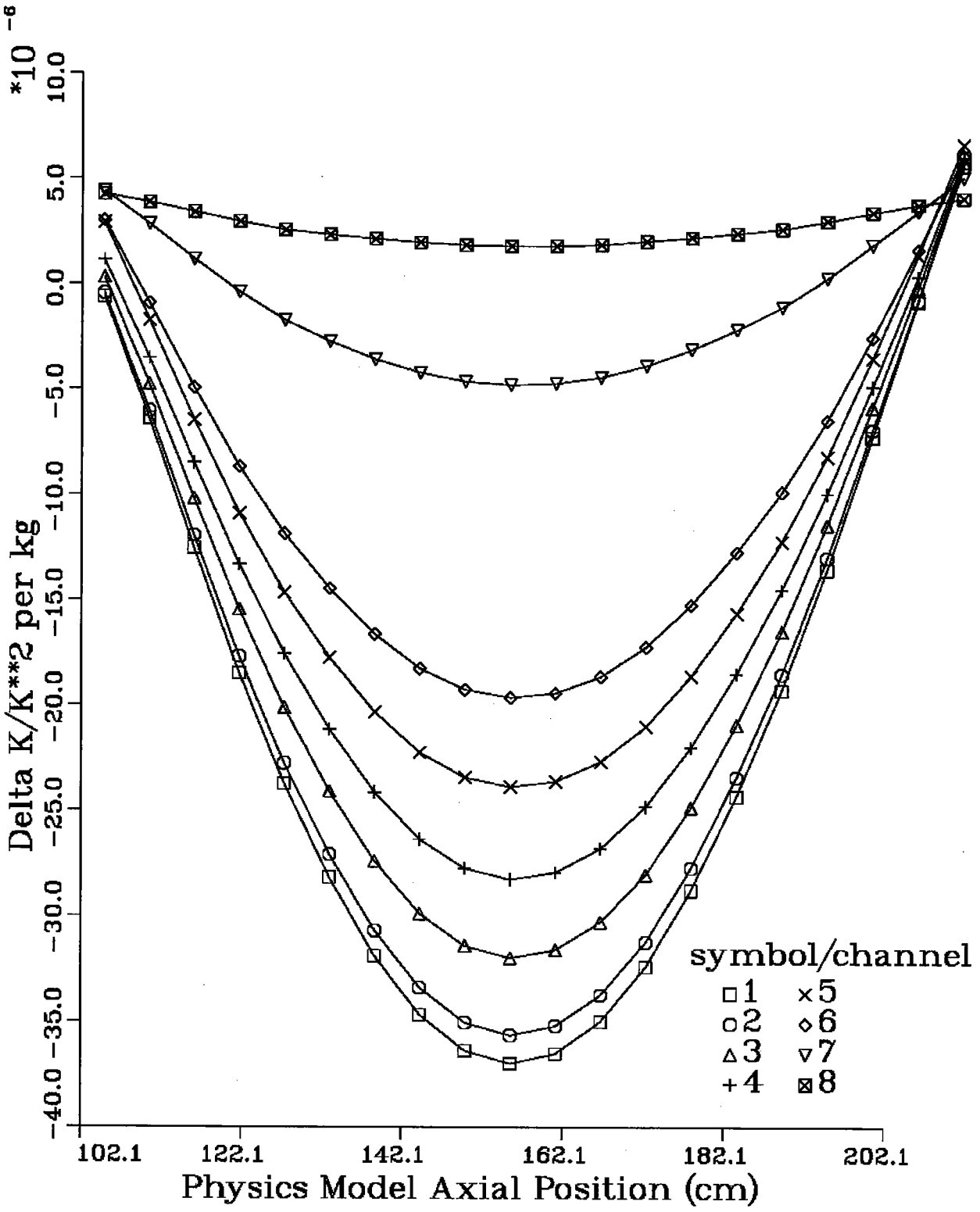

Figure 5. Structure Density Worth

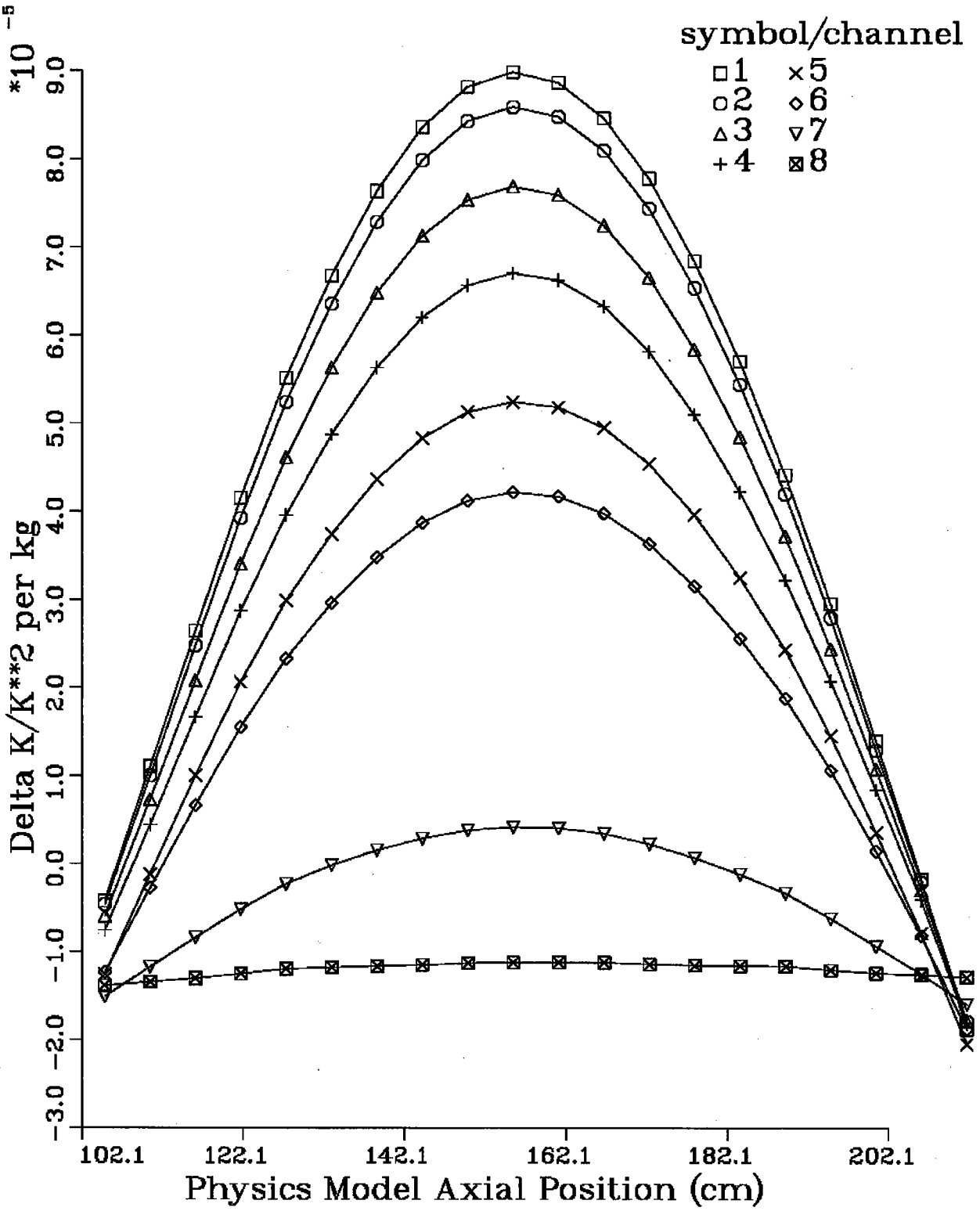

Figure 6. Sodium Density Worth

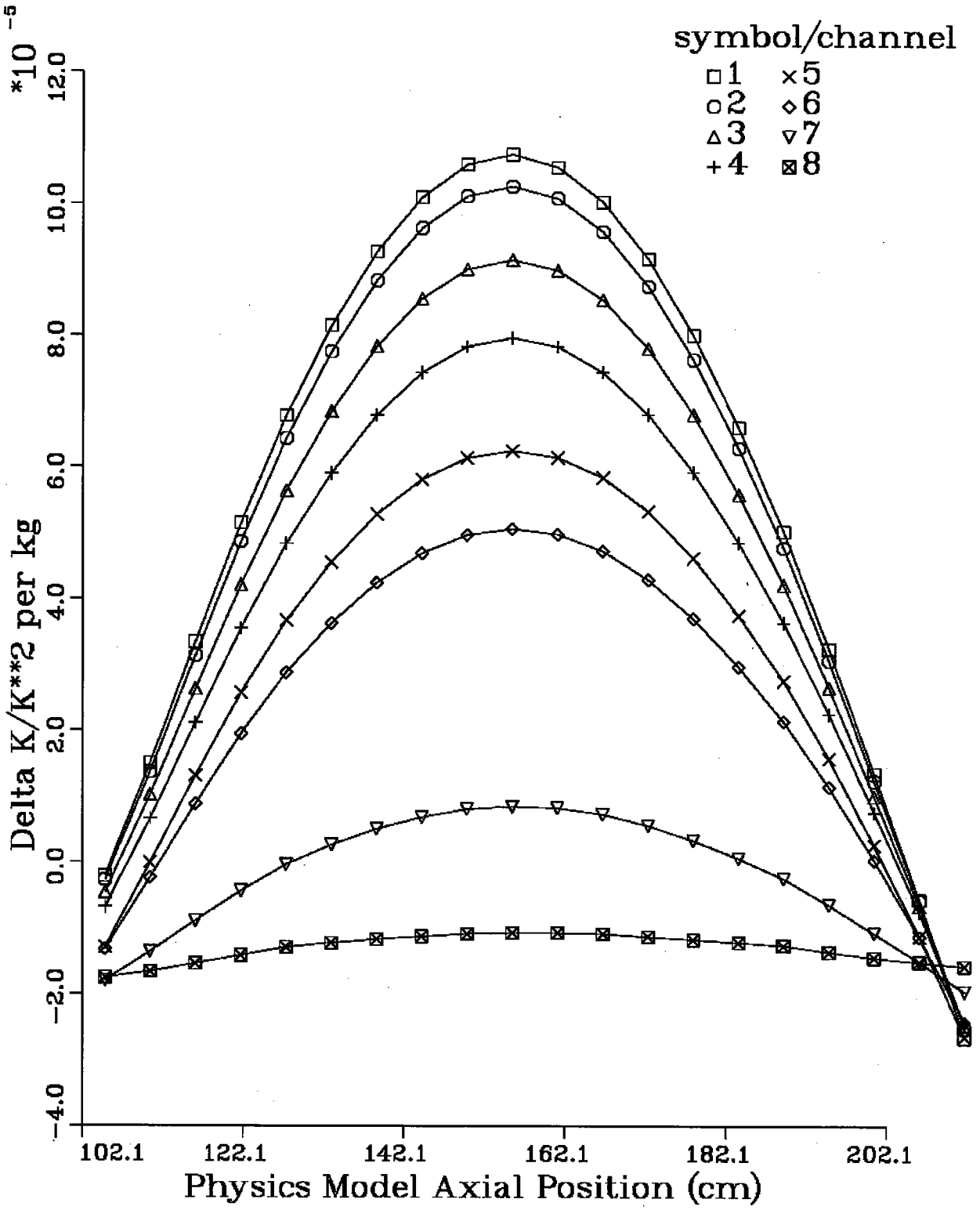

Figure 7. Sodium Void Worth

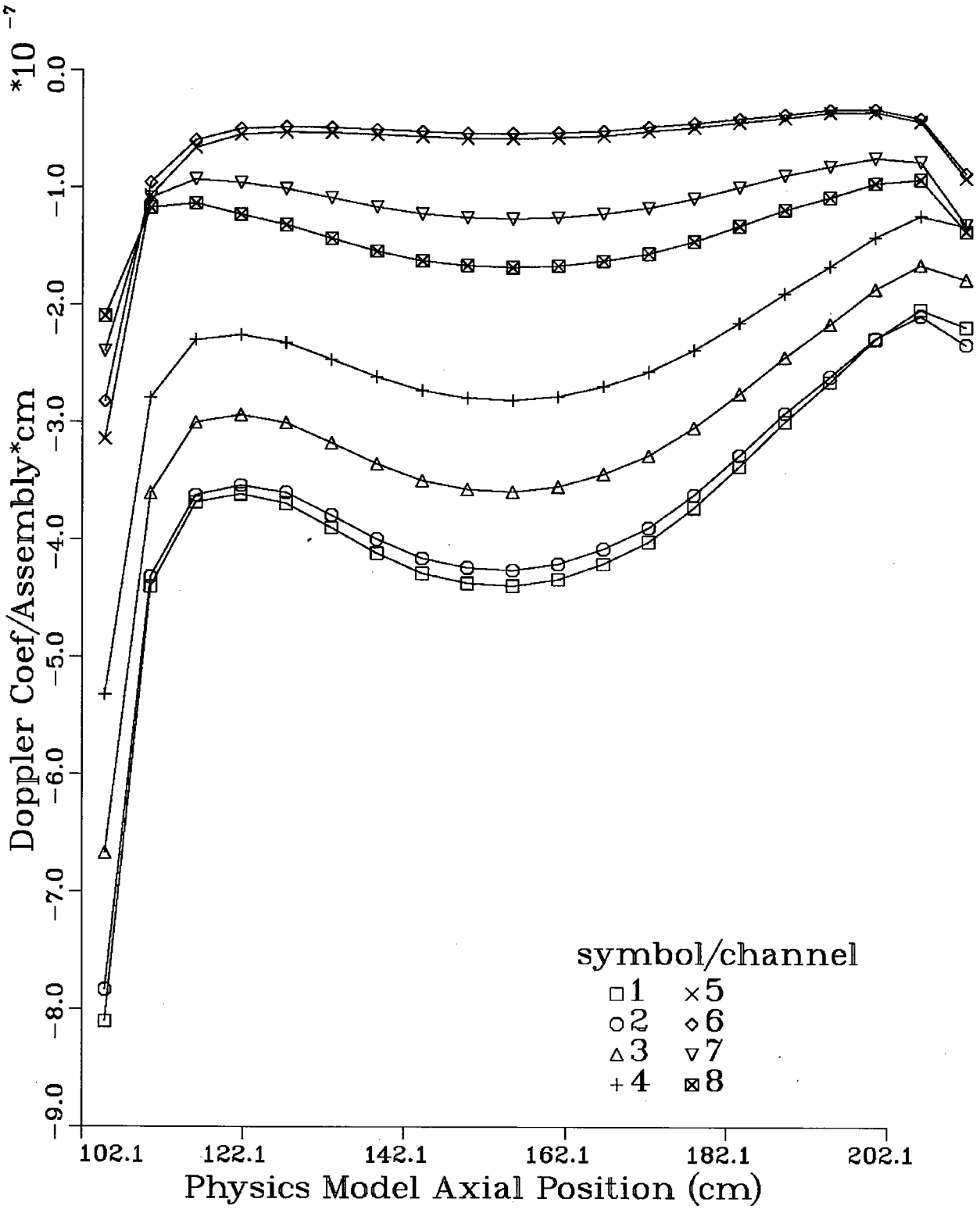

Figure 8. Flooded Doppler Worth

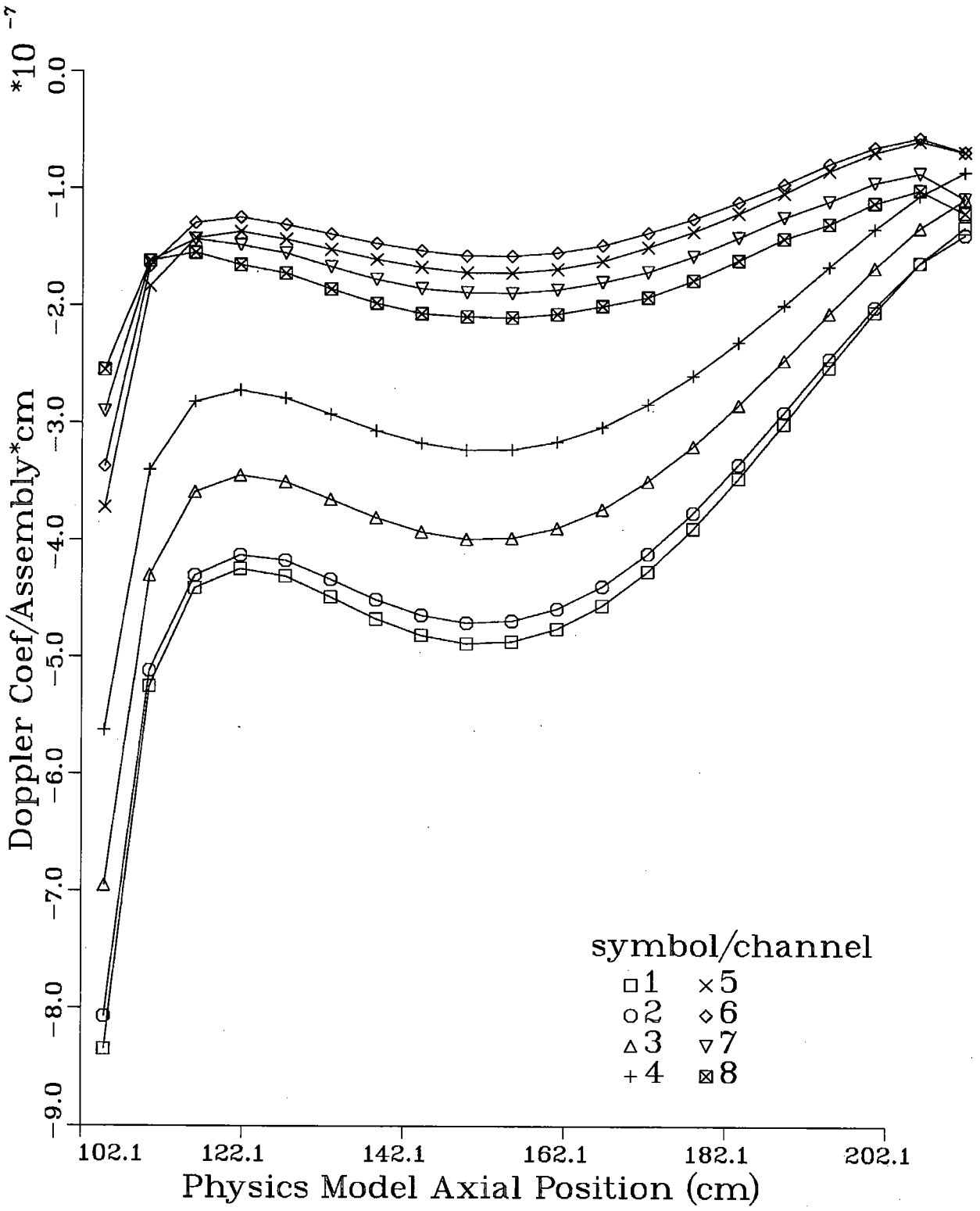

Figure 9. Voided Core Doppler Worth

VII. Conclusions

Parametric studies were performed for variations of the core geometry and fuel assembly design. Although earlier studies [2] showed that low conversion ratios could be achieved by using a high leakage core geometry, the large core diameter is undesirable from an economical point of view. In this work it has been shown that the same low conversion ratios can also be obtained using a compact core design. However, the compact core has the disadvantage of a shorter operating cycle and increased peak linear power. Core performance parameters for the low conversion ratio designs appear feasible, however, questions still remain to be answered on the ability to manufacture and utilize the highly enriched fuel required (~50% TRU) and the impact of the higher peak linear power and sodium void worth.

A more rigorous investigation of the reactivity coefficients was performed using transport theory. All of the coefficients except for the sodium void worth were found to be modeled accurately using diffusion theory. The errors in the sodium void worth were overcome by modifying the cross section generation approach and a conservative estimate of the sodium void worth was obtained using diffusion theory.

A 0.25 conversion ratio configuration of the compact core design was chosen as the system point design for this work. Both a startup scenario and recycle scenario were investigated. When compared to previous work, all of the calculated reactivity coefficients for the compact core appear to indicate that they will not have an adverse impact upon the accident scenarios considered. Overall, the most important penalty incurred by the low conversion ratio reactors is the increased burnup reactivity loss. If further investigation indicates that the burnup reactivity loss is unacceptably high, this penalty could be mitigated by reducing the cycle length.

References

1. R. N. Hill, D. C. Wade, J. R. Liaw, and E. K. Fujita, "Physics Studies of Weapons Plutonium Disposition in the Integral Fast Reactor Closed Fuel Cycle," Nuclear Science and Engineering, **121**, 17 (1995).

2. M. A. Smith, E. E. Morris, and R. N. Hill, "Physics and Safety Studies of Low Conversion Ratio Sodium Cooled Fast Reactors," GLOBAL 2003, Nov. 16-20, New Orleans, LA, 2003.

3. H. Henryson II, B. J. Toppel, and C. G. Stenberg, "MC2-2: A Code to Calculated Fast Neutron Spectra and Multigroup Cross Sections," ANL-8144, Argonne National Laboratory (1976).

4. B. J. Toppel, " A User's Guide to the REBUS-3 Fuel Cycle Analysis Capability," ANL-83-2, Argonne National Laboratory (1983).

5. R. D. Lawrence, "The DIF3D Nodal Neutronics Option for Two- and Three-Dimensional Diffusion Theory Calculations in Hexagonal Geometry," ANL-83-1, Argonne National Laboratory (1983).

6. C. H. Adams, "Specifications for VARI3D—A Multidimensional Reactor Design Sensitivity Code," FRA-TM-74, Argonne National Laboratory (1975).

7. "The SAS4A/SASSYS-1 LMR Analysis Code System," Argonne National Laboratory Report, ANL-FRA-1996-3 (August 1996).

8. C. H. Adams, "TOSAS4A, Newsletter No. 3," Argonne National Laboratory Internal Memo, May 18, 1988.

9. Blomquist, R.N., "VIM- A Continuous Energy Neutronics and Photon Transport Code," Int. Topl. Mtg. Adv. In Mathematics, Computations and Reactor Physics, April 28-May 2, 1992, Pittsburgh, PA.

10. T. Fanning, private communication; Argonne National Laboratory (January 2003).

11. R. N. Hill & R. N. Blomquist, private communication; Argonne National Laboratory (January 2003).

12. J. E. Quinn, P. M. Magee, M. L. Thompson, and T. Wu, "ALMR Fuel Cycle Flexibility," Proc. American Power Conf., Chicago, Illinois, April 13-15, 1993, Vol. 55, p. 1079, Illinois Institute of Technology (1993).

13. G. Palmiotti, E. E. Lewis, C. B. Carrico, "VARIANT: VARIational Anisotropic Nodal Transport for Multidimensional Cartesian and Hexagonal Geometry Calculation," *Argonne National Laboratory* ANL-95/40, 1995.

14. R. N. Hill, et. al. "Multiple Tier Fuel Cycle Studies for Waste Transmutation," ICONE 10, April 14-18, Arlington, VA, 2002.

Nuclear Engineering Division
Argonne National Laboratory
9700 South Cass Avenue, Bldg. 208
Argonne, IL 60439-4842

www.anl.gov

A U.S. Department of Energy laboratory managed by The University of Chicago